Geophys. J. Int. (1993) **115**, 159–167

Possible shallow crustal shear wave anisotropy off Lofoten, Norway, inferred from three-component ocean-bottom seismographs

Rolf Mjelde and Markvard A. Sellevoll
Institute of Solid Earth Physics, University of Bergen, Allégt. 41, 5007 Bergen, Norway

Accepted 1993 March 3. Received 1993 March 1; in original form 1992 October 5

SUMMARY

P- and *S*-wave velocity models along two perpendicular profiles 145 and 175 km long on the undrilled continental shelf off Lofoten, northern Norway, have been obtained from the study of nine three-component ocean bottom seismographs.

A V_P/V_S ratio of 1.96–2.15 is found in the sedimentary layers along a NE–SW profile. These high values are consistent with shaly sediments, which are identified in dredged bedrock samples. Along a NW–SE profile the *S*-wave velocities in the sedimentary layers are 5–10 per cent higher than along a NE–SW profile. The most likely explanation for this velocity difference is seismic anisotropy, which might be caused by liquid-filled microfractures alligned along the direction of the present-day maximum horizontal compressive stress.

The V_P/V_S ratio in the upper crystalline crust is found to be 1.75 along both profiles. If the inferred anisotropy described above is caused by aligned microcracks, the lack of anisotropy in the crystalline basement indicates that these cracks are restricted to the sedimentary layers. It must be emphasized, however, that the observed azimuthal difference in *S*-wave velocities could be caused by lateral velocity variations in the sediments, although the anisotropy hypothesis is considered more likely.

Key words: continental margin crust, seismic anisotropy, three-component ocean bottom seismographs.

INTRODUCTION

Studies of seismic data traditionally have been, and are still, concentrated mostly on compressional (*P*) waves. This is related to the fact that *P* waves alone often have been regarded as satisfactory for analysing geological aspects in regional geodynamic studies as well as in prospecting.

Other wave modes have often been regarded as noise, both because the *P* waves largely provide the desired geological information, and because the high-amplitude level of the *P* waves often dominates the wave train to such a degree that interpretation and effective use of later arriving wave modes can be hampered by large uncertainties.

It has, however, been understood that numerous geological problems can be elucidated in more detail by an integrated use of shear (*S*) and *P* waves than by study of *P* waves alone. An example illustrating this is the better constraints that can be found on possible lithologies if the *S*-wave velocity is known in addition to the *P*-wave velocity. An integrated use of *S* and *P* waves can further indicate whether a possible reservoir is gas or water saturated. This is related to the fact that the shear modulus (μ) of a rock is independent of the fluid in the pores, which causes the gas-saturated rock to have a slightly higher *S*-wave velocity than a completely water-saturated rock, since gas has lower density (ρ) than water. The *P*-wave velocity, however generally will be significantly lower in a gas-saturated then in a water-saturated rock because the *P*-wave velocity, in addition to being a function of μ and ρ, also is a function of the bulk modulus (k), which depends on the fluid in the pores (Tatham & Stoffa 1976).

Other interesting aspects of *S* waves are their sensitivity to systematic orientation of cracks and microcracks, indicated through numerous observations of *S*-wave splitting (Crampin 1990), and their possible sensitivity to preferred orientations of minerals and grains.

Such aspects, together with the improvements of seismic sources, three-component receivers, and processing, interpretation and modelling techniques, have strengthened the view that *S* waves in many cases can, and should, be studied both in detail and in combination with *P* waves. An

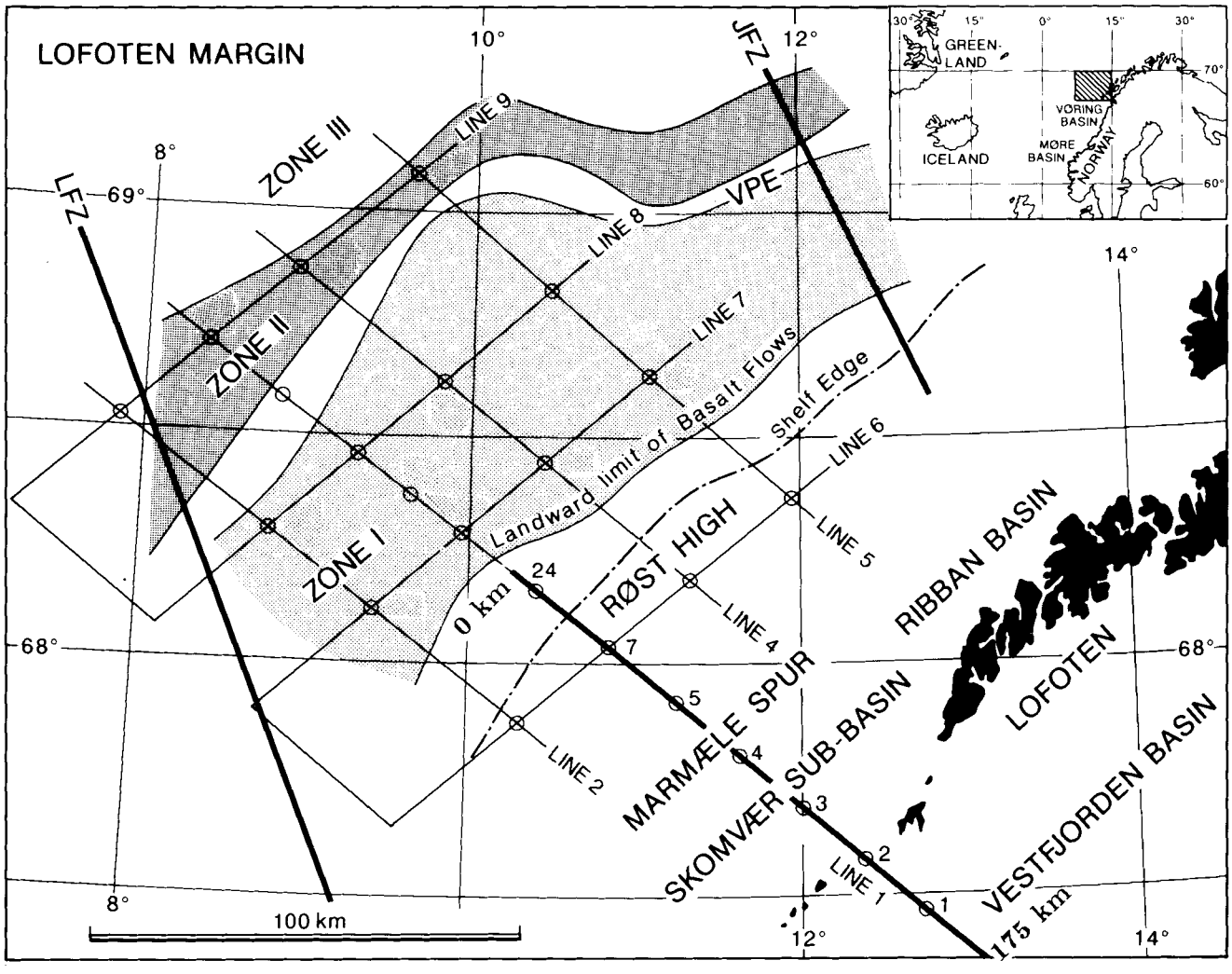

Figure 1. Main structural elements off Lofoten with positions of OBSs (circles) and seismic reflection and refraction profiles (lines 1–9) shot during the 1988 survey indicated. The position of the seismic reflection profile shot by GECO in 1987 (line 1) and described in this paper is indicated as a heavy line. VPE, the northward continuation of the Vøring escarpment; LFZ, Lofoten lineament; JFZ, Jennegga lineament; ZONE I, early Eocene flood-baslat; ZONE II, seaward dipping reflectors; ZONE III, oceanic crust. The position of the Vøring and Møre basins are indicated in the upper right corner. Modified from Sellevoll (1988).

extensive crustal experiment incorporating the study of *S* waves was performed in 1988 off Lofoten, northern Norway (Mjelde *et al.* 1992). In that survey, 24 three-component ocean bottom seismographs (OBSs) covering the area from continental shelf to oceanic crust were used (Fig. 1).

A 2-D *P*- and *S*-wave velocity model along a profile shot on the continental shelf (line 6; Fig. 1) was presented by Mjelde (1992). In that study it was shown that incorporating *S* waves in the analysis enabled conclusions to be made concerning the lithology of the sediments.

The present paper describes the 2-D *P*- and *S*-wave velocity model in the sediments and upper crystalline crust along profile 1 in Fig. 1. The data from this profile are of the same high quality as those of the profile previously studied, and the analysis of profile 1 could contribute to verifying and constraining the conclusions drawn in Mjelde (1992). In addition, the two profiles are perpendicular, which should enable possible azimuthal anisotropy to be detected.

GEOLOGICAL FRAMEWORK

The region (Fig. 1) was characterized by a compressional regime in the late Silurian to early Devonian, resulting in suturing of the Laurentia (Greenland) and Baltica (Scandinavia) plates and the formation of the Caledonides (Bøen, Eggen & Vollset 1984; Bukovics *et al.* 1984; Gage & Dore 1986). The crystalline basement in Lofoten is believed to represent an exhumed deep section of the continental crust (Chroston & Brooks 1989).

No boreholes have been drilled on the Lofoten margin, and the present model of this margin (Mokhtari 1991) has been based primarily on the gross stratigraphic relationships observed along the shelf. The margin has been dominated by extensional tectonics in post-Caledonian time, and pre-Cretaceous sequences with a maximum thickness of about 5 km in the Vestfjorden basin are present along most of the shelf (Mjelde *et al.* 1993).

The late Jurassic to early Cretaceous extension led to major faulting activity along the entire margin, partly as reactivation of older fault zones, generally creating slightly rotated fault blocks and causing subsequent subsidence along major rift systems (Rønnevik, Eggen & Vollset 1983; Bøen *et al.* 1984; Hinz, Dostman & Hanisch 1984; Mutter 1984; Skogseid & Eldholm 1989; Mokhtari 1991). Thick sedimentary sequences of Cretaceous age are preserved on the Lofoten shelf; within the Ribban Basin (Fig. 1) they locally exceed 5 km in thickness.

The early Cainozoic extension axis shifted westward with respect to the Jurassic–Cretaceous episode, and finally caused continental separation in the earliest Eocene. Tertiary sediments are very thin or absent over the Lofoten shelf. It is uncertain whether Palaeogene sediments have been eroded by post-depositional uplift or whether the shelf remained emergent during this period. The Lofoten shelf appears to have been a sediment bypass area in the Neogene.

DATA ACQUISITION

Acquisition of the OBS data was performed during the summer of 1988 using *R/V Håkon Mosby*, University of Bergen. The scientific programme comprised seismic reflection, seismic refraction and gravimetric measurements performed simultaneously. The positions of the seismic reflection and refraction lines and ocean bottom seismographs (OBSs) are indicated in Fig. 1.

Four Bolt 1500 C air-guns with a total volume of 79 l (4800 in.^{3}) were used as the source array. The guns were towed at a depth of 21 m and the shotpoint interval was 240 m (2 min).

The OBS instruments used were developed and built by the geophysical institutes at the Hokkaido and Tokyo Universities (Shimamura 1988). The analogue OBS instruments have three orthogonal components (4.5 Hz gimbal mounted geophones), one vertical and two horizontal. The instruments can record continuously for 14 days within the frequency range from 1 to 30 Hz (−3 dB).

Twenty-four OBS instruments were used to acquire the seismic refraction data, of which seven were located at 20–25 km intervals along the profile described in this paper (Fig. 1). Unfortunately, the magnetic tapes from OBS 2 were blank; the acquisition thus provided wide-angle data from 6 OBS instruments located along the studied profile. The analysis of the data from the remaining profiles is presented in Mjelde (1992) and Mjelde *et al.* (1992, 1993).

DATA PROCESSING

Velocity filtering and several deconvolution schemes have been applied to the OBS data (digitized at the Hokkaido and Tokyo universities) to help identify the phase and the onset of the different *S*-wave phases, as described in Mjelde (1992). However, the quality of the raw data is excellent, and the data examples presented in this paper have been bandpass filtered (6–13 Hz) only. The data are plotted with Automatic Gain Control (4 s window), and the interpretation of the data is carried out on displays with traveltime reduced by 8 km s^{-1}.

RESULTS AND DISCUSSION

Figure 2 shows the seismogram from the vertical component of OBS 7 (from Mjelde *et al.* 1993), and Figs 3–6 show the seismograms from one of the horizontal components of OBS 7 and 5. Calculated traveltimes indicated in Figs 4 and 6 represent critical refractions (head waves) plotted beyond the critical angle. Only one of the horizontal components is presented since both (non-reoriented) horizontal components are apparently very similar. The lower quality of the *S*-wave arrivals on the vertical component seismograms (Fig. 2) indicates that the *S* waves can be interpreted and modelled in a more reliable way by studying the horizontal components.

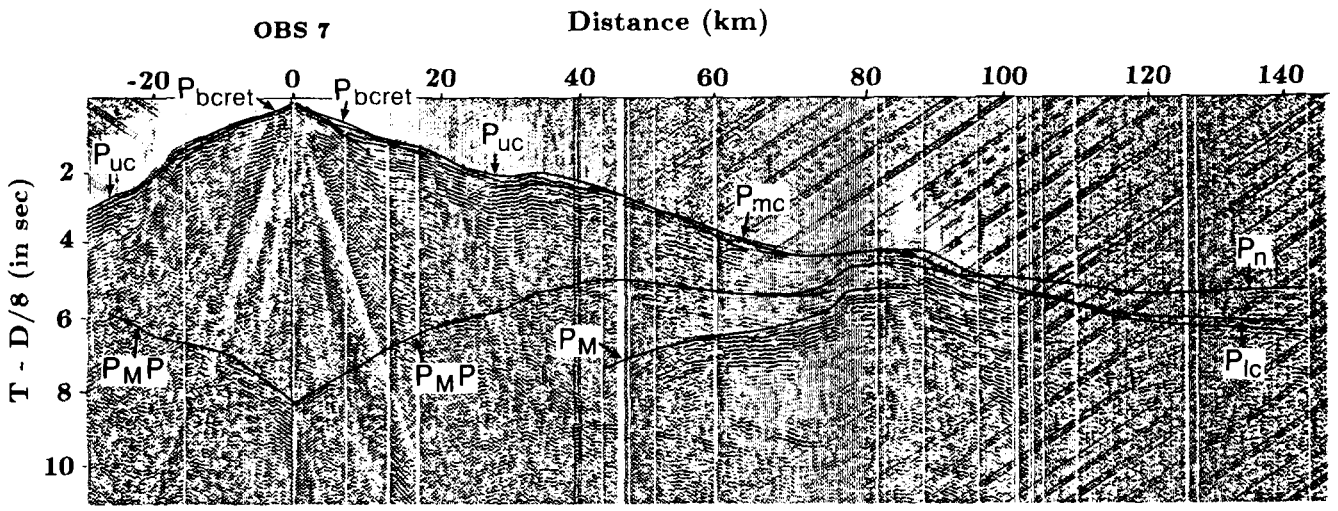

Figure 2. OBS 7 vertical component with traveltime curves calculated from the model in Fig. 7 (from 2-D ray tracing) indicated. P_{bcret}, base of Cretaceous refraction; P_{uc}, upper crust refraction; P_{mc}, middle crust refraction; P_{lc}, lower crust refraction; P_n, Moho refraction; P_MP, Moho reflection; P_M, upper mantle reflection.

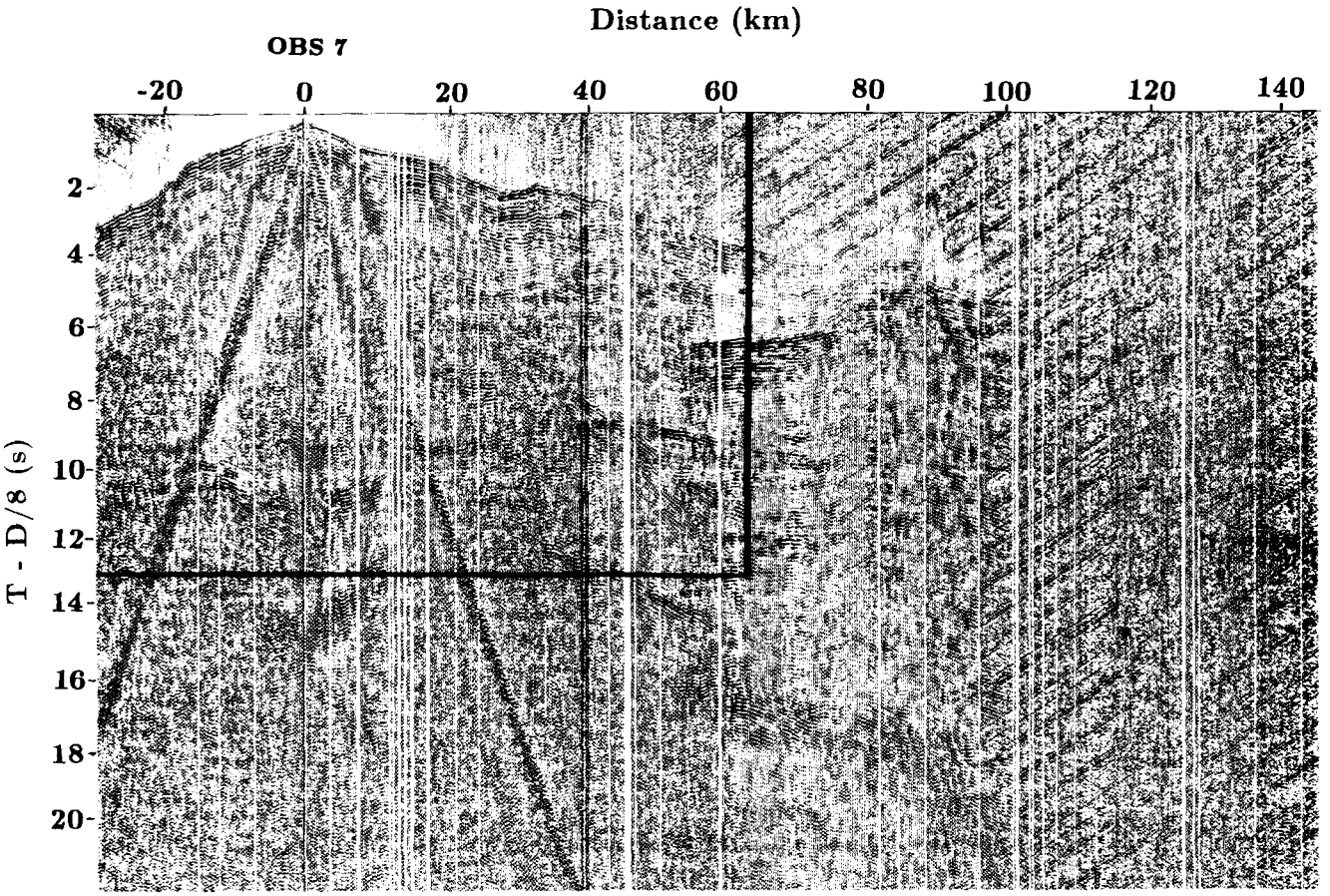

Figure 3. OBS 7 horizontal component (reduction velocity 8.0 km s^{-1}). 6–13 Hz bandpass filtered. A close-up of the framed area is shown in Fig. 4.

The *P*-wave model

Figure 7 shows the *P*-wave model (Mjelde *et al.* 1993) and the V_P/V_S ratio for the profile calculated from 2-D kinematic ray tracing. The uncertainty in the Moho depth and velocities (both *P* and *S*) for this model is estimated to be ±1 km and ±0.1 km s^{-1} respectively, implying a maximum uncertainty in the V_P/V_S ratio of ±0.2. A more detailed uncertainty analysis is described in Mjelde *et al.* (1992).

The crustal structure along the profile is characterized by a succession of basement highs and deep basins. Sequences of Tertiary sediments are thin and partially absent along the profile. Three Cretaceous sequences (early, middle and late Cretaceous) are identified with *P*-wave velocities of 2.7 km s^{-1}, 3.1 km s^{-1} and 4.0 km s^{-1} respectively. The 5.1 km s^{-1} refractor coincides with the base of the Cretaceous reflector interpreted and mapped in detail on the shelf by Mokhtari, Pegrum & Sellevoll (1989). The thickness of the pre-Cretaceous sediments varies considerably along the profile, with a maximum thickness of about 5 km in the Vestfjorden Basin south-east of OBS 1.

The 6.0 km s^{-1} refractor is interpreted to represent the top of crystalline (continental) basement. The crystalline crust is divided into three layers: an upper, an intermediate and a lower crustal layer, with *P*-wave velocities of 6.0 km s^{-1}, 6.4 km s^{-1} and 6.8 km s^{-1} respectively. The velocity below the Moho is measured at 8.2 km s^{-1}.

The sedimentary, crystalline crustal and upper mantle *P*-wave velocities along this profile are the same as those found along the perpendicular profile (line 6, Mjelde *et al.* 1992). This implies either isotropic *P*-wave propagation along these two azimuths, or that possible *P*-wave anisotropy is too modest to be detected (less than about 3 per cent). The absence of the 2.7 km s^{-1} and 4.0 km s^{-1} layers along line 6 indicates that the amounts of late and early Cretaceous sediments on the north-western part of the shelf are insignificant. This is confirmed from the modelling of line 1 and from studies of multichannel reflection data (Mokhtari 1991).

The V_P/V_S model in the sediments

The *P*-wave model, which is described in detail by Mjelde *et al.* (1993), was used as a basis for modelling the *S* waves described in the present paper. The V_P/V_S ratios that best satisfy the observations are indicated in Fig. 7. As in the modelling of line 6 (Mjelde 1992) we assume that the waves are *P*-to-*S* converted at the sea-floor, which represents a very high impedance contrast (the thickness of the Tertiary sediments is negligible along the entire profile).

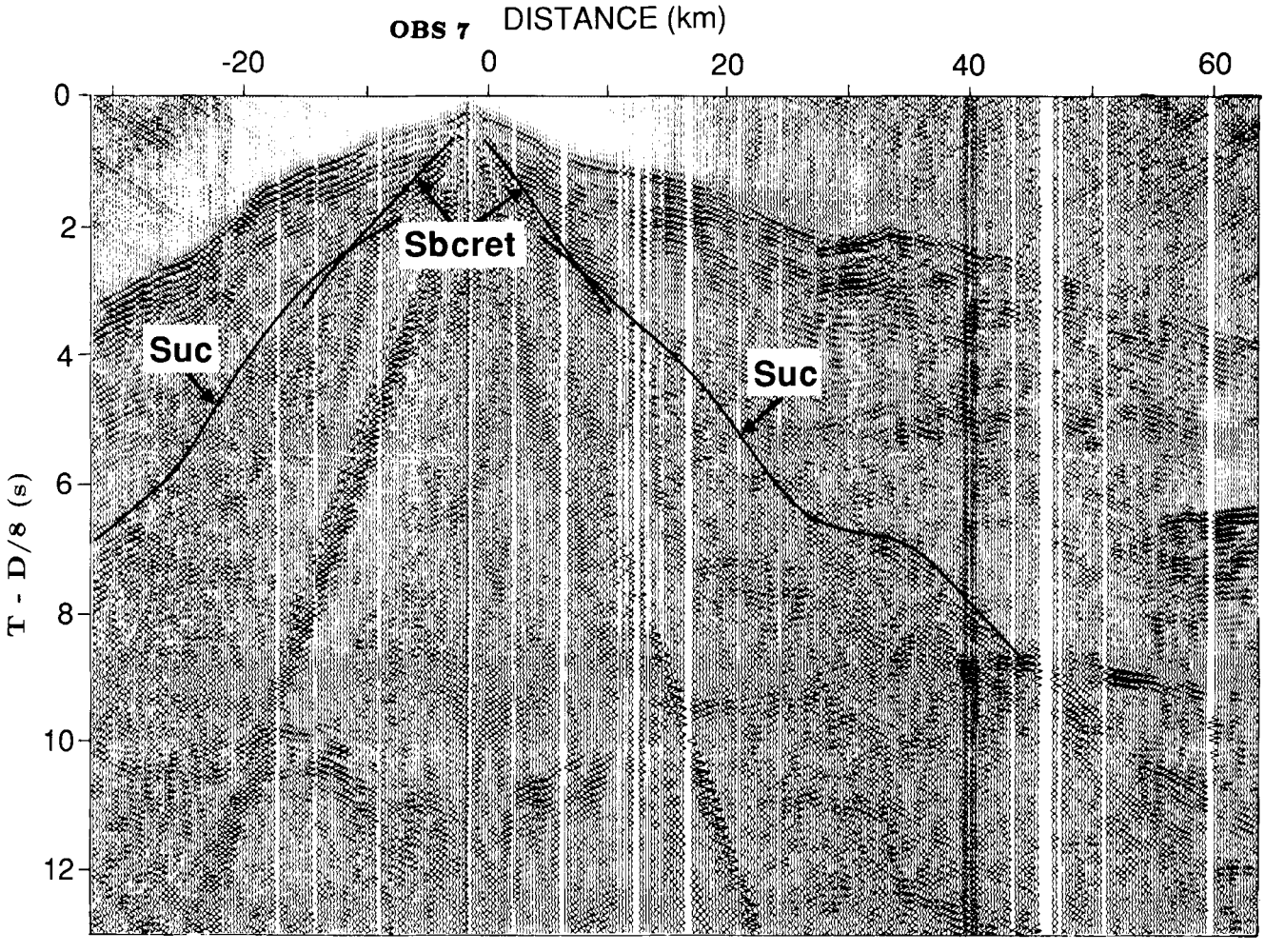

Figure 4. Part of OBS 7 horizontal component (see Fig. 3) with traveltime curves from the model in Fig. 7 indicated (calculated from 2-D ray tracing). S_{bcret}, base of Cretaceous refraction; S_{uc}, upper crust refraction.

The *S*-wave modelling along line 6 indicated a V_P/V_S ratio of 2.15 (Vs = 1.4 km s^{-1}) in the Cretaceous sediments, and a V_P/V_S ratio of 1.95 (Vs = 2.6 km s^{-1}) in the pre-Cretaceous sediments. Mjelde (1992) concluded that these high ratios indicated shaly sediments which is consistent with observations from bedrock samples dredged from the sea-floor (Løseth *et al.* 1989). In the south-western part of the profile (south of the Røst High) the *S*-wave velocity in the sediments were found to be higher than on the Røst High, probably as a result of lateral lithology variations. Such lateral heterogeneity was not observed on the Røst High over a lateral distance of more than 50 km.

The modelling along line 1 (Fig. 7) indicates a V_P/V_S ratio of 2.0 (Vs = 1.35 km s^{-1}), 1.95 (Vs = 1.59 km s^{-1}) and 1.9 (Vs = 2.11 km s^{-1}) in the three Cretaceous sedimentary sequences respectively, and a V_P/V_S ratio of 1.85 (Vs = 2.76 km s^{-1}) in the pre-Cretaceous sediments. The mean V_P/V_S ratio of 1.95 in the Cretaceous sediments is confirmed from the intercept time for the critical refraction along the base of the Cretaceous. The vertical decrease in the V_P/V_S ratio from the Cretaceous to the pre-Cretaceous sediments can most likely be explained by decreasing porosity and microfracturing with depth in the shaly sediments, although vertical lithology variations cannot be excluded.

The modelling thus indicates that the *S*-wave velocity in the Cretaceous and pre-Cretaceous sedimentary layers are, respectively, about 0.19 km s^{-1} and 0.16 km s^{-1} higher along line 1 than along the perpendicular profile. The most likely explanation for this azimuthal velocity difference is seismic anisotropy; the modelling indicates that this possible *S*-wave anisotropy is at least 10 per cent in the Cretaceous sequence, and about 5 per cent in the pre-Cretaceous sediments. It is important to notice that the layers with Cretaceous sediments are very thin under OBS 7 where the two profiles cross. The significant thickness of the pre-Cretaceous sediments assures, however, a reliable estimate of the inferred anisotropy for these oldest sediments. The homogeneous velocity distribution in the Cretaceous sequence (mainly middle Cretaceous) over at least 50 km lateral distance to the north-east of OBS 7 along line 6 (low velocity) and beneath OBS 3 and 5 along line 1 (high velocity), together with the results from dredged bedrock samples (Løseth *et al.* 1989), suggest that the observed velocity difference between the two profiles is due to anisotropy for the Cretaceous sediments also, and not to

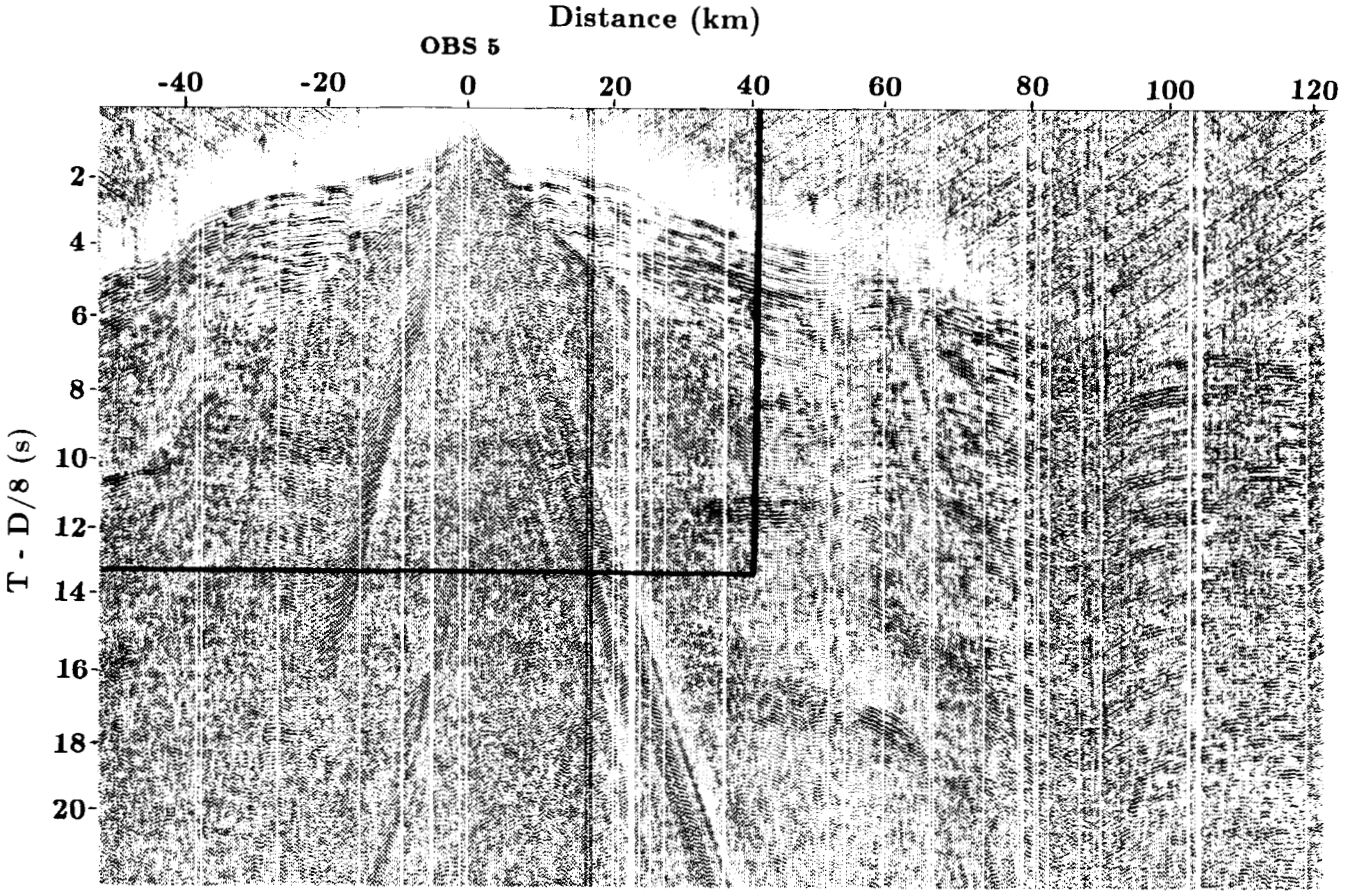

Figure 5. OBS 5 horizontal component (reduction velocity 8.0 km s^{-1}). 6–13 Hz bandpass filtered. A close-up of the framed area is shown in Fig. 6.

lateral heterogeneity. It is clear, however, that this inferred anisotropy for the Cretaceous sediments is not very well constrained.

It is unlikely that the cause of the inferred anisotropy is related to the large-scale crustal structures, fine-scale layering or alignment of minerals, since observable *P*-wave anisotropy would be expected in this case. To our knowledge, the only possible explanation for an *S*-wave anisotropy being at least three times higher than the *P*-wave anisotropy (which is needed to explain the observations in the OBS data) is the presence of fluids in some form of aligned cracks and pores. A simple and plausible model that explains the possible anisotropy inferred from our data is liquid-filled microcracks aligned along the direction of the present-day maximum horizontal compressive stress. In Fig. 8 it is shown that the direction of the *P* axes of fault plane solutions interpreted by Bungum *et al.* (1990) to represent the direction of maximum compressive stress in northern Norway and in the Lofoten region, strike NW–SE, which is close to the azimuth of profile 1 where the high *S*-wave velocities are observed. The fact that significantly different velocities are measured for the first-arriving *S* waves along the two perpendicular directions indicates that the profiles are shot very close to, respectively, the fast and slow directions of the inferred anisotropic medium. If the profiles had been acquired along oblique azimuths with regard to these axes of symmetry, each generated *S* wave (*SV* wave) would have split into two *S* wave polarized parallel, and perpendicular, to the microcracks respectively. In this case the same velocity (fast) would have been measured for the first-arriving *S* wave along both profiles, and the inferred anisotropy could only have been studied by use of more sophisticated methods.

In the Cretaceous sediments the inferred 10 per cent anisotropy might be explained by a model consisting of vertically aligned penny-shaped liquid-filled microcracks with a crack density (CD) of 0.1 ($CD = Na^3/v$, where N is the number of cracks of radius a and half-thickness d in volume v) and aspect ratio (AR) of 0.05 ($AR = d/a$) (Fig. 9). The ray-tracing modelling indicates that the possible anisotropy in the sediments decreases with depth, which is consistent with the assumption of decreasing crack density with increasing confining pressure (depth). *S*-wave anisotropy of this kind inferred to be related to the present-day stress-field has been reported frequently during the last few years, and it has been argued that such anisotropy is more or less omnipresent in the upper 10–20 km of the crust (Crampin 1990).

It is important to emphasize that a small amount of anisotropy with a vertical axis of symmetry, which is commonly observed in shales (e.g. Jones & Wang 1981; Banik 1984; Johnston & Christensen 1992), might be present in the area. However, presence of a significant amount of such anisotropy (5 per cent or higher) would have

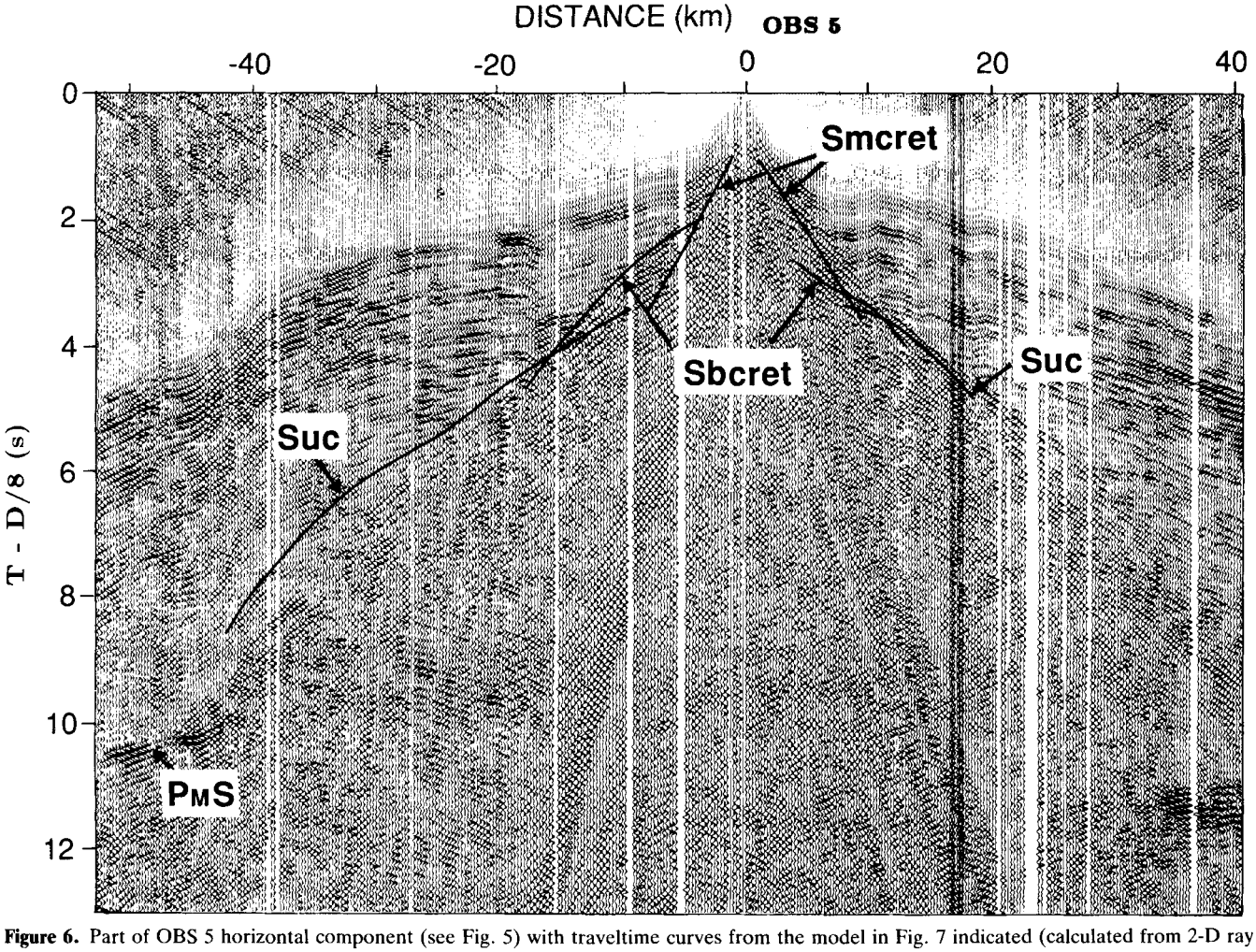

Figure 6. Part of OBS 5 horizontal component (see Fig. 5) with traveltime curves from the model in Fig. 7 indicated (calculated from 2-D ray tracing). S_{mcret}, middle Cretaceous refraction; S_{bcret}, base of Cretaceous refraction; S_{uc}, upper crust refraction; P_MS, mode conversion at the Moho.

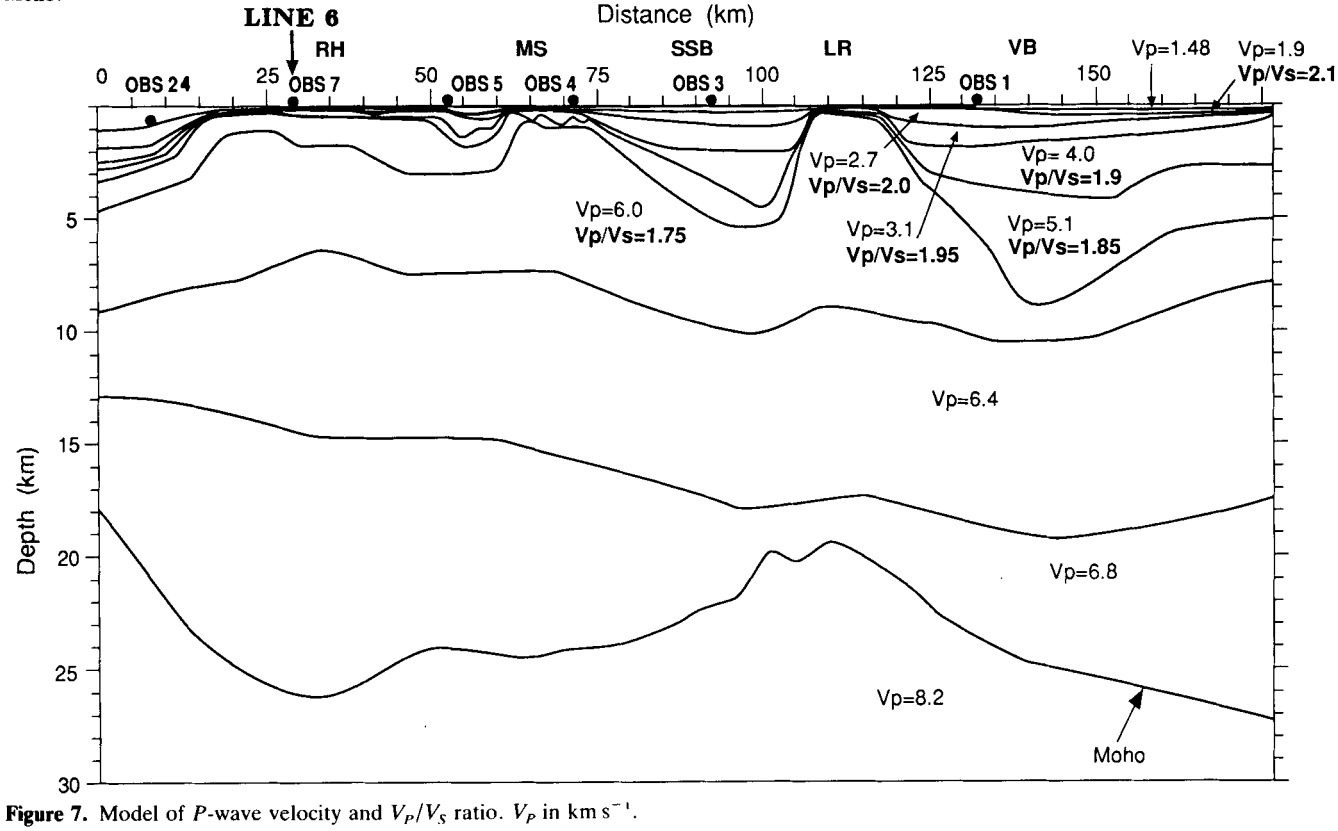

Figure 7. Model of P-wave velocity and V_P/V_S ratio. V_P in km s^{-1}.

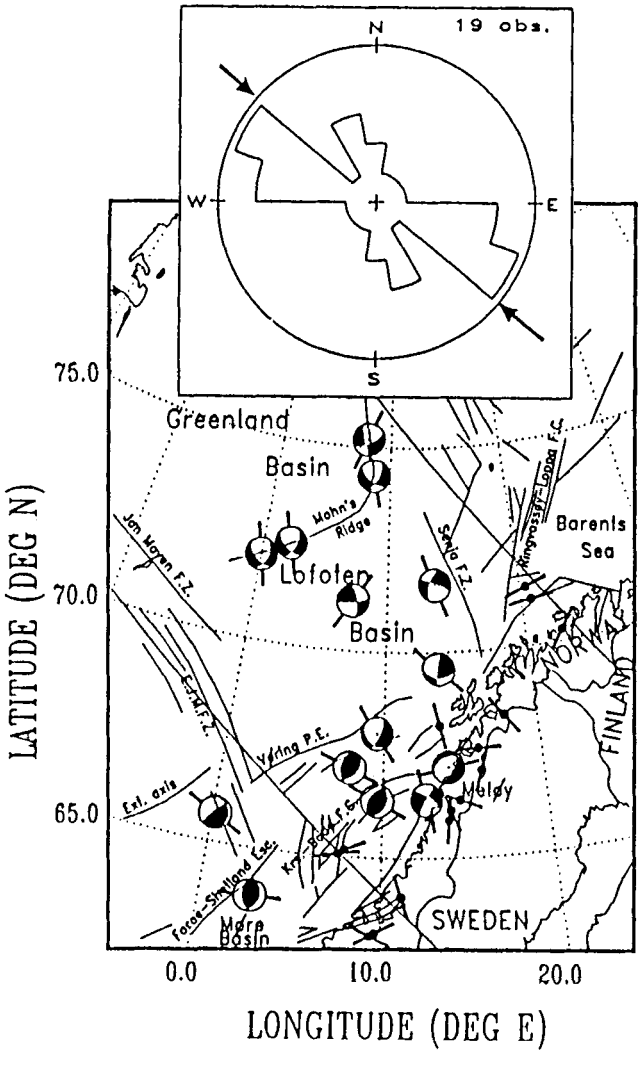

Figure 8. Focal mechanism solutions and *in situ* stress measurements (solid circles) in the region. The lines (bars) through the focal sphere projections indicate the directions of the *P* axes (maximum compressive stress). The two parallel NW–SE trending lines across the map are 'ridge push' directions. The rose diagram shows the maximum compressive stress directions from earthquakes in northern Norway and the Svalbard areas. Arrows indicate the approximate 'ridge push' direction. (From Bungum *et al.* 1990.)

been revealed during the modelling of both the *P* waves and the *S* waves, since the OBS data contain information from arrivals propagating both horizontally and near vertically in all layers.

We must emphasize that a conclusion that the observed difference in *S*-wave velocities for the two profiles could be caused by lateral velocity variations in the sediments cannot be excluded. This interpretation would imply that the sediments on the landward side of the Røst High (profile 6) might be interpreted as being more sandy than those on the Røst High, since sandy sediments generally have a lower V_P/V_S ratio than shale (Neidell 1985; Mjelde 1992). The discussion above, however, demonstrates that the anisotropy hypothesis must be considered as more likely.

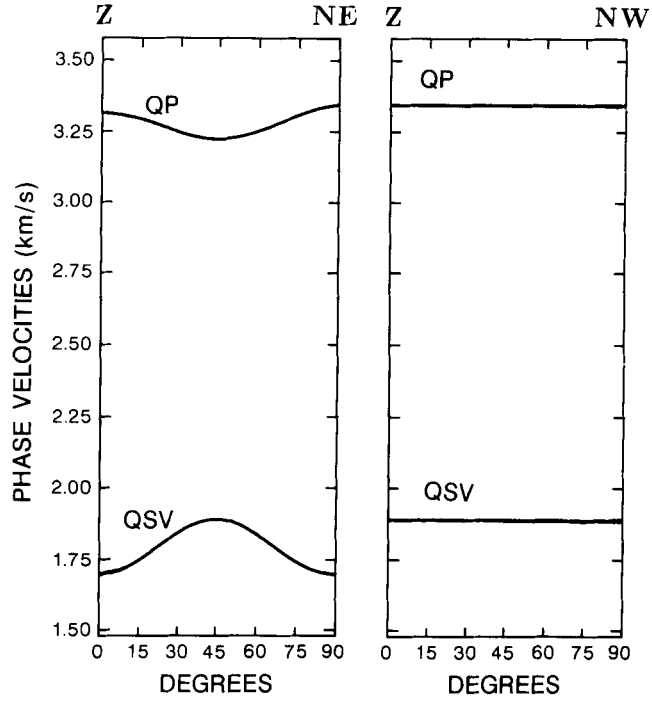

Figure 9. Variation of theoretical phase velocities with direction of propagation for quasi-*P* waves and quasi-*SV* waves propagating through parallel liquid-filled microcracks aligned vertically and striking NW–SE (along profile 1) (penny-shaped cracks with crack density 0.1 and aspect ratio 0.05). Modified from Crampin (1978).

The *S*-wave model in the upper crystalline crust

The V_P/V_S ratio in the upper crystalline crust is found to be 1.75 ($Vs = 3.4\,km\,s^{-1}$), which is consistent with the velocities found along line 6. If the inferred anisotropy described above is caused by aligned microcracks, the lack of anisotropy in the crystalline basement indicates that these cracks are restricted to the sedimentary layers, or that they close at shallow depths in the crystalline basement; from about 2 to 5 km. This is consistent with laboratory measurements (Nur & Simmons 1969; Chroston & Brooks 1989) and the fact that the inferred anisotropy is observed to decrease with depth in the sediments. The observations are not, however, consistent with estimates of *S*-wave anisotropy in some other areas, where these microcracks have been inferred to remain open down to at least 10 km depth (Crampin 1990). The reason for this difference remains to be found, but the inferred shallow closure on the Lofoten continental shelf might be related to early Tertiary uplift of the shelf resulting in upward migration of fluids.

CONCLUSIONS

A consistent *S*-wave velocity model along two perpendicular profiles (Fig. 1, profiles 1 and 6) on the continental shelf off Lofoten, northern Norway, has been obtained by studying the horizontal components of nine OBSs. The V_P/V_S ratio in the sedimentary layers decreases vertically, probably as a result of decreasing porosity and microfracturing with depth in the shaly sediments.

The S-wave velocity in the sedimentary layers is significantly higher along the NW–SE profile (profile 1) than along the perpendicular profile (profile 6). The most likely explanation for this azimuthal velocity difference is anisotropy; the ray-tracing modelling indicates that the possible S-wave anisotropy is about 10 per cent in the Cretaceous sequence, and about 5 per cent in the pre-Cretaceous sediments. One possible cause of this inferred anisotropy might be liquid-filled microfractures aligned along the direction of the present-day maximum compressive stress.

The V_P/V_S ratio in the upper crystalline crust is found to be 1.75 along both profiles. If the inferred anisotropy described above is caused by aligned microcracks, the lack of anisotropy in the crystalline basement indicates that these cracks are restricted to the sedimentary layers, or that they close at relatively shallow depths (2–5 km) in the crystalline basement. This is consistent with what is generally observed in laboratory measurements, and the fact that the inferred anisotropy is observed to decrease with depth in the sediments. The observations are not, however, consistent with estimates of S-wave anisotropy in some other areas, where such microcracks have been inferred to remain open down to at least 10 km depth.

It must be emphasized, however, that it cannot be excluded that the observed azimuthal difference in S-wave velocities might be caused by lateral velocity variations in the sediments, although we find the anisotropy hypothesis more likely. Performing a new seismic experiment using more closely spaced seismographs would be necessary to allow discrimination between the two hypothesis.

ACKNOWLEDGMENTS

The authors thank Professor H. Shimamura, Dr T. Iwasaki (Laboratory for Ocean Bottom Seismology, University of Hokkaido) and Professor T. Kanazawa (Laboratory for Earthquake Chemistry, University of Tokyo) for providing instruments and indispensable help during the acquisition and pre-processing of the data, and Professor R. Kanestrøm [Norsk Hydro and Institute of Solid Earth Physics (IFF), University of Bergen (UiB)] and Dr C. Hurich (IFF, UiB) for fruitful comments on the manuscript.

We also thank Statoil for financial support and help; in particular we would like to thank E. W. Berg, V. B. Larsen, L. B. Pedersen and K. J. Skaar.

REFERENCES

Banik, N. C., 1984. Velocity anisotropy of shales and depth estimation in the North Sea basin, *Geophysics*, **49,** 1411–1419.

Bukovics, C., Shaw, N. D., Cartier, E. G. & Ziegler, P. A., 1984. Structure and development of the mid-Norway continental margin, in *Petroleum Geology of the North European Margin*, pp. 407–423, ed. Spencer, A. M. *et al.*, Graham and Trotman, London.

Bungum, H., Alsaker, A., Kvamme, L. B. & Hansen, R. A., 1990. Seismicity and seismotectonics of Norway and nearby continental shelf areas, *J. geophys. Res.*, **96, B2,** 2249–2265.

Bøen, F., Eggen, S. & Vollset, J., 1984. Structures and basins of the margin from 62–69°N and their development, in *Petroleum Geology of the North European Margin*, pp. 3–28, ed. Spencer, A. M. *et al.*, Graham and Trotman, London.

Chroston, P. N. & Brooks, S. G., 1989. Lower crustal seismic velocities from Lofoten–Vesterålen, north Norway, *Tectonophysics*, **157,** 251–269.

Crampin, S., 1978. Seismic wave propagation through a cracked solid: polarization as a possible dilatancy diagnostic, *Geophys. J. R. astr. Soc.*, **53,** 467–496.

Crampin, S., 1990. The scattering of S waves in the crust, *Pageoph*, **132,** 67–91.

Gage, M. S. & Dore, A. G., 1986. A regional geological perspective of the Norwegian offshore exploration provinces, in *Habitat of Hydrocarbons on the Norwegian Continental Shelf*, pp. 21–38, Norwegian Petroleum Society, Graham and Trotman, London.

Hinz, K., Dostman, H. J. & Hanisch, J., 1984. Structural elements of the Norwegian Sea continental margin, *Geol. Jahrb.*, **A75,** 193–211.

Johnston, J. E. & Christensen, N. I., 1992. Shear wave reflectivity, anisotropies, Poisson's ratios and densities of a southern Appalachian Paleozoic sedimentary sequence, *Tectonophysics*, **210,** 1–20.

Jones, L. E. A. & Wang, H. F. 1981. Ultrasonic velocities in Cretaceous shales from the Williston basin, *Geophysics*, **46,** 288–297.

Løseth, H., Hansen, J. W., Århus, N., Weiss, H. M. & Rokoengen, K., 1989. Palynological dating and organic geochemistry of bedrock samples off Lofoten and Vesterålen, *IKU report No. 24.1504.00/01/89.*

Mjelde, R., 1992. Shear waves from three-component ocean bottom seismographs off Lofoten, Norway, indicative of anisotropy in the lower crust, *Geophys. J. Int.*, **110,** 283–296.

Mjelde, R., Sellevoll, M. A., Shimamura, H., Iwasaki, T. & Kanazawa, T., 1992. A crustal study off Lofoten, N. Norway, by use of 3-component ocean bottom seismographs, *Tectonophysics*, **212,** 269–288.

Mjelde, R., Sellevoll, M. A., Shimamura, H., Iwasaki, T. & Kanazawa, T., 1993. Crustal structure beneath Lofoten, N. Norway, from vertical incidence and wide-angle seismic data, *Geophys. J. Int.*, **114,** 116–126.

Mokhtari, M., 1991. A geological model for the Lofoten continental margin, *DSc thesis*, IFF, University of Bergen.

Mokhtari, M., Pegrum, R. M. & Sellevoll, M. A., 1989. A geophysical study of the Norwegian continental margin between 67°N and 69°N, *SEISMO-SERIES*, **28,** IFF, University of Bergen.

Mutter, J. C., 1984. Cenozoic and late mesozoic stratigraphy and subsidence history of the Norwegian Margin, *Bull. geol. Soc. Am.*, **95,** 1135–1149.

Neidell, N. S., 1985. Land application of S waves, *Geophysics: The Leading Edge of Exploration*, **11,** 32–44.

Nur, A. & Simmons, G., 1969. Stress-induced velocity anisotropy in rock: an experimental study, *J. geophys. Res.*, **74,** 6667–6674.

Rønnevik, H. C., Eggen, S. & Vollset, J., 1983. Exploration of the Norwegian Shelf, in *Petroleum Geochemistry and Exploration of Europe*, pp. 71–94, ed. Brooks, J., Blackwell Scientific Publications, Oxford.

Sellevoll, M. A., 1988. Seismiske undersøkelser av Lofoten Marginen og refleksjonsseismiske test-målinger på Mohns Rygg, M/S Håkon Mosby, 29 juli–19 august 1988, *Toktrapport*, IFF, University of Bergen.

Shimamura, H., 1988. *OBS technical description*, Vedlegg til Toktrapport, Sellevoll, 1988.

Skogseid, J. & Eldholm, O., 1989. Vøring Plateau continental margin: seismic interpretation, stratigraphy and vertical movements, in *Proceedings of the Ocean Drilling Program, Scientific Results*, Vol. 104, pp. 993–1030, ed. Eldholm, O., Thiede, J. & Taylor, E., Ocean Drilling Program, College Station, TX.

Tatham, R. H. & Stoffa, P. L., 1976. V_P/V_S—a potential hydrocarbon indicator, *Geophysics*, **41,** 837–849.